

Characterization of key magnetohydrodynamic phenomena in PbLi flows for the US DCLL blanket

Sergey Smolentsev^{a,*}, René Moreau^b, Mohamed Abdou^a

^a University of California, Los Angeles, USA

^b Laboratoire SIMAP, Groupe EPM, Grenoble - INP, France

ARTICLE INFO

Article history:

Received 17 April 2008

Received in revised form 7 July 2008

Accepted 16 July 2008

Available online 6 September 2008

Keywords:

Liquid metal blanket

Magnetohydrodynamic effects

Turbulence

Buoyant flows

ABSTRACT

The dual-coolant lead–lithium (DCLL) blanket concept is considered in the US for testing in ITER and as a candidate for using in DEMO reactor. In this blanket, the eutectic alloy lead–lithium circulates slowly as a coolant and breeder in the presence of a strong plasma-confining magnetic field, experiencing magnetohydrodynamic (MHD) effects. This paper overviews the ongoing studies for the MHD flows in the US DCLL blanket, focusing mostly on the poloidal flows where most of the volumetric heating is deposited and the MHD effects are therefore of primary importance. The paper introduces qualitative description of MHD flows in the blanket along with mathematical models and numerical and analytical results to address such phenomena as the near-wall jet formation, quasi-two-dimensional MHD turbulence, and buoyant flows. Special consideration is given to the buoyancy effects in the buoyancy-opposed flows, where superposition of forced and buoyant flows may lead to locally reverse or recirculation flows. The present analysis suggests that such flows are possible both in ITER and DEMO scenarios. We also discuss conditions when the poloidal flows in the blanket turn to be turbulent.

© 2008 Elsevier B.V. All rights reserved.

1. Introduction

In a liquid metal (LM) blanket, either lithium (Li) or eutectic alloy lead–lithium (PbLi) circulates as a breeder (*e.g.* helium-cooled lead–lithium (HCLL) blanket [1]) or as a breeder and a coolant (*e.g.* dual-coolant blanket [2], self-cooled blanket [3]). The LM motion in a strong reactor plasma-confining magnetic field induces an electric current, which in turn interacts with the magnetic field, resulting in the volumetric Lorentz force, which has a strong effect on the LM flow field, and through modifications of the flow, on heat and mass transfer. Such flows, known as magnetohydrodynamic (MHD) flows, have been the subject of intensive studies for many decades in many practical areas, including metallurgical applications, crystal growth, MHD pumps, MHD flow meters, MHD ship propulsion, *etc.* (see examples in Ref. [4]). As applied to a blanket, MHD flows occur in a complex fusion environment, including strong multi-component spatially- and time-varying magnetic fields, complex geometry and multi-material domains. The magnetic field has a primary effect on the blanket performance and its thermal efficiency via changes in the velocity/electric current distribution, pressure drop and heat and mass transport. Above all, the MHD phenom-

ena in a fusion blanket owe their uniqueness to the presence of a high-intensity neutron flux, causing volumetric heating and driving associated buoyant flows.

At present, understanding the underlying physics of MHD flows and their impact on the blanket performance remain far from being complete even at a qualitative level. Addressing MHD phenomena under blanket-relevant conditions is difficult due to their non-linearity, multi-scale nature, and complex blanket geometry. Full numerical simulations for real geometry flows are often limited to relatively low values of operation parameters, *e.g.* magnetic field strength. The experimental limitations are caused by the requirements for a large magnet workspace, strong prototypic magnetic fields and prototypic neutron sources, the conditions that can hardly be met at the same time in non-fusion devices. All these make studying MHD phenomena in the blanket conditions very challenging.

In the recent past, several overviews of LM MHD flows in fusion-relevant conditions were presented, focusing on the blanket issues common to all types of LM blankets, such as the MHD pressure drop, flow distribution, electrical insulation, complex geometry flows, effects due to magnetic field non-uniformity, multi-channel (Madaramé) effect, heat transfer, *etc.* [5–8]. A few papers have overviewed specific issues associated with concrete blanket designs (*e.g.* [9,10]). The main goal of the present paper is to summarize the most important MHD results obtained in the course of the ongoing LM blanket studies in the US for the so-called

* Corresponding author at: UCLA, MAE, 43-133 Engineering IV, Los Angeles, CA 90095-1597, USA. Tel.: +1 310 794 5366; fax: +1 310 825 2599.

E-mail address: sergey@fusion.ucla.edu (S. Smolentsev).

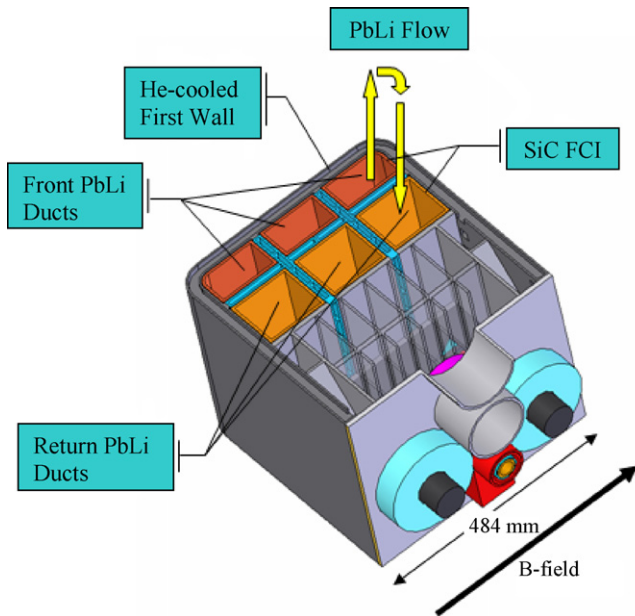


Fig. 1. Sketch of the US ITER DCLL test blanket module.

DCLL (dual-coolant lead–lithium) blanket, which is considered for testing in ITER and as a candidate for using in DEMO reactor. In this effort, we try to give the overall physical picture of the unique MHD phenomena in this type of blankets. The interested reader can find further details in Refs. [11–16]. Special emphasis is given to buoyancy-driven and turbulent flows, which are expected to dominate in the DCLL blanket conditions, but have not been sufficiently presented in the previous overviews. Here, we focus mostly on the flows in the poloidal ducts where almost all blanket power is deposited and the MHD effects on the flow and heat transfer are therefore of primary importance. Although the paper is mostly intended as an overview, we also introduce for the first time our initial analysis for mixed convection when the forced flow is downward (buoyancy-opposed flow) as such flows occur in many (if not all) poloidal blanket designs, where the LM makes several poloidal passes when moving from the blanket inlet to the outlet.

2. US DCLL blanket

The DCLL blanket concept evolved from the original ARIES studies [17] is considered in the US for testing in ITER (Fig. 1) and as a primary candidate for a DEMO reactor (Fig. 2) [18,19]. In the DCLL blanket, eutectic alloy PbLi circulates slowly (~ 10 cm/s) for power conversion and tritium breeding. Reduced activation ferritic steel is used as the structural material and helium (He) is used to cool the first wall and the blanket structure. At present, the US efforts in developing the DCLL blanket for DEMO are limited to the reactor outboard. In what follows we refer to the outboard DEMO blanket as a DEMO design. The overall geometry of the blanket modules in ITER and DEMO is similar but the number of poloidal ducts and cross-sectional dimensions are different. The poloidal length in both cases is about 2 m, while the radial depth is smaller in ITER TBM. The module box is strengthened by helium-cooled vertical stiffening plates (grid plates) connecting the first wall panel with a strong back wall. There are additional stiffening plates (separation walls) to separate the two (in ITER blanket) or three (in DEMO blanket) rows of poloidal ducts and to support the side walls of the external box. The liquid metal enters the inlet manifold at the bottom of the blanket module from the annulus of the concentric pipe and from

there is distributed into three (in ITER blanket) or four (in DEMO blanket) front poloidal ducts where it flows upwards. At the top of the module, the PbLi makes a 180° turn and then flows downwards through the return ducts at the back of the module. At the bottom of the module, the liquid is collected and leaves the module from the outlet manifold through the internal tube of the concentric pipe.¹

A key element of the DCLL concept is the flow channel insert (FCI) made of silicon carbide (SiC), either as a composite or as foam, which serves as electrical insulator to reduce the impact from the MHD pressure drop of the circulating liquid metal, and as thermal insulator to separate the high temperature PbLi from the ferritic structure (Fig. 3). Using FCIs allows for high exit temperature (700°C or even higher) and may lead to high blanket efficiency making this design very attractive for future studies as suggested first in Ref. [20]. The FCI is separated from the ferritic wall by a thin (~ 2 mm) gap also filled with PbLi. Both the gap flow and that inside the FCI box (bulk flow) are driven by the same pressure head. The gap and the bulk flows are connected through small openings made in one of the FCI walls (either holes or a slot). The optimum location of the openings has been analyzed in Ref. [12]. The openings may be needed for equalizing the pressure on both sides of the FCI. The flow inserts in the poloidal ducts are segmented into a few 20–50 cm sections overlapping at the juncture similar to the roof tiles. The blanket thermal efficiency is strongly dependent on insulating properties (electrical and thermal) of the FCI. The desirable blanket configuration requires minimization of heat leakages from the PbLi flows into He streams as well as minimization of the MHD pressure drop, while keeping the interface temperature between the PbLi and the ferritic structure and the temperature drop across the FCI below the allowable limits. Meeting all these requirements places special limitations on the FCI design and SiC properties, such as electrical (σ_{SiC}) and thermal (k_{SiC}) conductivity as discussed in Ref. [12]. At present, two FCI designs are underway: a single-layer FCI and a double-layer (nested) FCI. In this paper, our considerations are limited to a simple single-layer FCI as shown in Figs. 1–3.

3. Dimensionless parameters in the poloidal flow

The MHD flows in the blanket ducts can generally be characterized by the following dimensionless parameters: the Hartmann number $Ha = B_0 L \sqrt{\sigma / (\nu \rho)}$ (Ha^2 is the ratio of the electromagnetic force to viscous force); the Reynolds number $Re = U_0 L / \nu$ (Re is the ratio of inertia to viscous force); and the Grashof number $Gr = g \beta \Delta T L^3 / \nu^2$ (represents the ratio between the buoyancy and viscous forces). Here, B_0 , L , U_0 and ΔT are the applied (toroidal) magnetic field, characteristic flow dimension, mean-flow velocity and characteristic temperature difference, while ρ , ν , σ , β and g stand for fluid density, kinematic viscosity, electrical conductivity, volumetric thermal expansion coefficient and acceleration of gravity correspondingly. Typical values of the dimensionless flow parameters in the poloidal duct flows (for the front ducts) are shown in Table 1. In the definition of Re and Gr , the duct half-width a (taken in the radial direction) is used as the length scale, while Ha is constructed using the Hartmann length b (half of the duct dimension in the toroidal direction). The characteristic temperature difference is defined through the average volumetric heating \bar{q} as $\Delta T = \bar{q} a^2 / k$, where k is the fluid thermal conductivity.

¹ At present, some blanket modifications are discussed in the US for both ITER and DEMO. In particular, an alternative flow scheme is suggested, where the PbLi flows first through the ducts at the back of the module. Also, using two separate pipes is currently considered to replace the single concentric pipe. These modifications are not considered here.

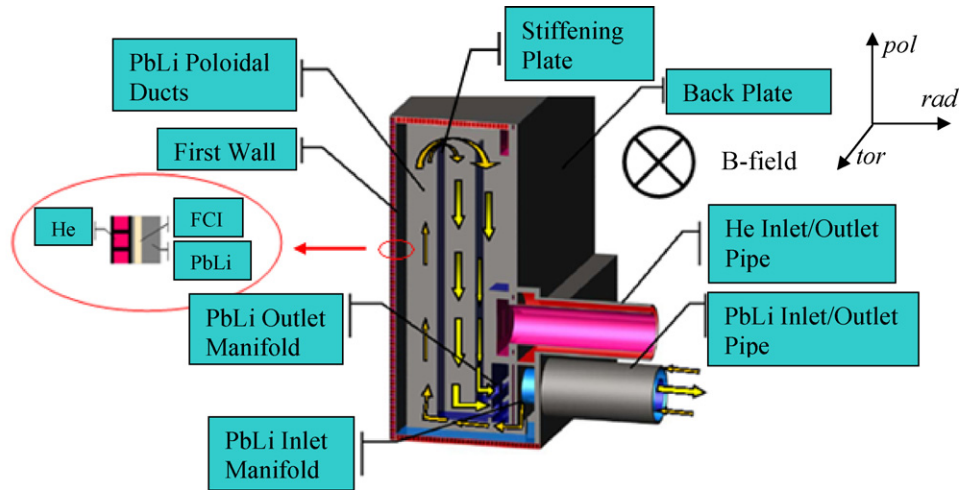


Fig. 2. Sketch of the US DCLL DEMO blanket module.

Typically, blanket flows exhibit very high Ha ($\sim 10^4$) and Gr (up to 10^{12}). The high values of Ha imply a special flow organization in rectangular ducts, namely, a near-uniform core and thin boundary layers at the walls: Hartmann layers whose thickness scales as b/Ha at the walls perpendicular to the magnetic field; and Shercliff (or side) layers at the other pair of walls, whose thickness scales as $b/Ha^{1/2}$. The extremely high values of Gr are quite typical of liquid metals, which are low Prandtl number fluids. Some combinations of the above parameters, such as Gr/Re^2 , Gr/Ha , Re/Ha , and $N = Ha^2/Re$ (Stuart number or interaction parameter), can also be useful when characterizing convective flows in the blanket. Parameter Gr/Re^2 (Archimedes number), which stands for the ratio between buoyancy and inertia forces, is much larger than unity, showing that buoyant flows can be dominating over inertia. Parameter Gr/Ha is also related to buoyant flows, namely when the temperature gradient is perpendicular to the magnetic field, as in the poloidal ducts. A large value of Gr/Ha indicates that in spite of the reduction of the buoyant velocity due to the

Hartmann damping, which includes both ohmic and viscous losses in the Hartmann layers, the buoyancy-driven flows are still pronounced. Parameter Re/Ha , which is the Reynolds number built through the thickness of the Hartmann layer, plays a fundamental role in the turbulence transitions. Namely, if Ha/Re is below or in the vicinity of its critical value $(Ha/Re)_{cr} \approx 1/300$ (e.g. [21,22]), turbulent flows are expected to be transitional from three-dimensional to quasi-two-dimensional (Q2D). In the blanket conditions, where $Ha/Re \gg (Ha/Re)_{cr}$, any originally three-dimensional turbulence is rapidly suppressed but turbulent flows are still possible in the special form of Q2D turbulence, which experience only a weak damping [23] and can persist over many eddy turnovers at a high-intensity level. It is often considered that high interaction numbers indicate small inertial effects in the momentum equation compared with the MHD effects. This is, however, partially true since in some cases, when the Hartmann walls are insulating or weakly conducting, the relevant ratio between the electromagnetic force and inertia is Ha/Re (e.g. [24]). In the past, a few approaches usu-

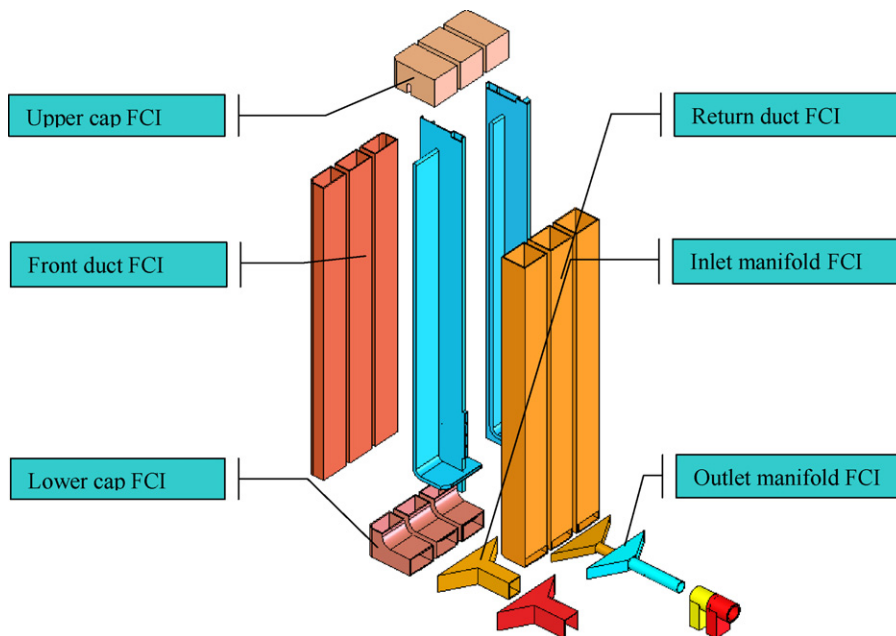


Fig. 3. Basic FCI configuration for ITER TBM. Pressure equalization openings are not shown.

ally called “core flow approximation” were developed for blanket applications based on the large values of N by neglecting the inertia terms and the viscous terms in the core (e.g. [25]).

4. Qualitative description of MHD phenomena in the DCLL blanket

Two types of induced electric current will circulate in the blanket. Cross-sectional currents are dominant in the long poloidal ducts, where the flow over the major length is expected to be about fully developed, demonstrating no or small variations along the flow path. These currents close their loop flowing through the FCI and then in the gap and the ferritic wall. The MHD pressure drop associated with the cross-sectional currents can be reduced by orders of magnitude through a proper choice of SiC by lowering its electrical conductivity or by making the FCI thicker. As shown in Ref. [12] under the DEMO blanket conditions, near-ideal electrical insulation can be achieved with a 5 mm FCI, providing $\sigma_{\text{SiC}} < 1 \text{ S/m}$.

In contrast to the poloidal flows, in such blanket elements as the inlet or outlet manifold or the coaxial pipe in the fringing magnetic field region, the flow is essentially three-dimensional. The major issues associated with the three-dimensional flows are related to high MHD pressure drop and flow distribution. In fact, most of the MHD pressure drop in the DCLL module is due to the three-dimensional flows [16]. Here, the MHD pressure drop and the velocity distribution are strongly affected by axial currents, which close their path mostly in the flow domain. Thus, in those blanket elements where the flow is essentially three-dimensional, the MHD drag cannot be reduced significantly using insulating flow inserts or other insulating techniques, and the FCI serves mostly as thermal insulator decoupling hot PbLi from the ferritic structure. A detailed review of blanket issues associated with the three-dimensional MHD pressure drop in complex geometry flows can be found in Ref. [5]. Current results of numerical simulations for prototypic three-dimensional flows under the DCLL blanket conditions computed with the newly developed MHD software called HIMAG are presented in Ref. [26] and important details of the numerical procedure itself are given in Ref. [27].

Depending on the flow parameters, FCI properties, heating conditions, etc., the poloidal flows (which are the main focus of this paper as stated in Section 1) will demonstrate either relatively simple or very complex behavior. In what follows we distinguish three DCLL blanket “scenarios,” namely: ITER H-H, ITER D-T and DEMO since the flow conditions for each scenario are very special. In the ITER H-H phase, volumetric heating is not applied. Even in the absence of volumetric heating some temperature differences in the flowing LM are possible (due to the applied surface heat flux and heat losses into the helium flows), but they seem to be too small to cause significant buoyancy effects compared with the forced flow. Therefore, in the ITER H-H scenario, the poloidal flows can be treated using a purely forced flow model. Unlike ITER H-H, in ITER D-T, and especially in DEMO, the neutron flux, being responsi-

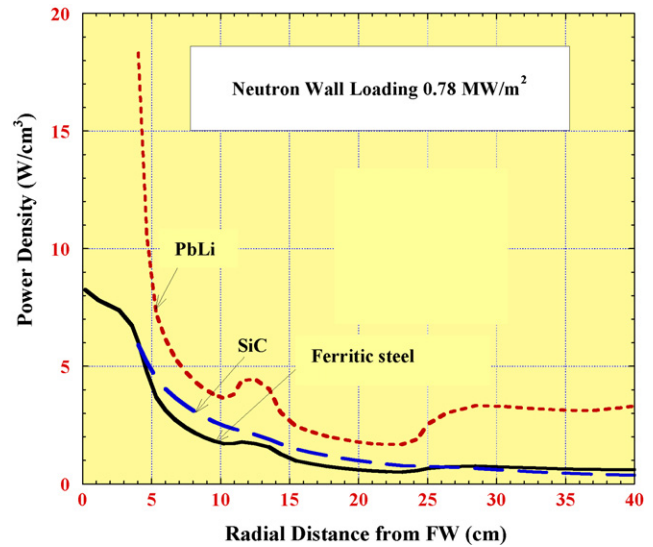


Fig. 4. Radial power density distribution in the ITER TBM associated with the high-intensity neutron flux [12].

ble for extremely high non-uniform volumetric heating (Fig. 4), is expected to drive buoyant flows whose intensity is comparable or even higher than that of the forced flow.

In ITER and DEMO, the Hartmann number is of the same order, while the Grashof number in DEMO is higher by about three orders of magnitude due to larger module dimensions and higher thermal loads. This suggests more intensive buoyant flows in DEMO compared with ITER. The complexity of the poloidal flows can also be affected by the FCI properties. Provided the electrical conductivity of the flow insert is very low, such that near-perfect insulation is achieved, the poloidal flows in the ITER H-H scenario seem to be relatively simple. Namely, all induced electric currents will close their path in the flow inside the FCI box through the Hartmann layers without crossing the FCI. Such currents are known to be responsible for the Lorentz force distribution resulting in a uniform velocity profile except for the thin boundary layers: the Hartmann and the side layers. These flows most likely do not produce turbulence; however, observing turbulence pulsations in the poloidal flows in these conditions is still possible as turbulence can be generated in the inlet manifold region and then transported from there into the poloidal flows without being significantly damped by the magnetic field. More complex flows are expected to occur in the conditions when the FCI is not perfectly insulating. In these conditions, the velocity profile is known to be “M-shaped,” whose characteristic feature is two high-velocity jets at the side walls. The most complex flows can, however, be foreseen in the ITER D-T and DEMO scenarios, where all possible MHD effects can appear at the same time. For example, the symmetry in the M-shaped velocity profile could be modified by the buoyancy-driven flows. The M-shaped velocity profiles, in turn, can be responsible for Q2D turbulence production. In the blanket conditions, such turbulence is of low damping due to its two-dimensionality and is favorable for intensive fluid mixing due to the presence of large coherent structures, thus affecting heat transfer and tritium transport. Taking into account that the convective transport in the blanket is essentially non-linear, the resultant flow may exhibit very unusual features, which are very difficult to predict.

As an additional complexity, one should mention significant temperature-dependent variations of the physical properties in both liquid and solid structure, which will affect the electric current distribution. Among other MHD effects, which might be important,

Table 1
Basic dimensionless flow parameters in the poloidal flow for ITER and DEMO

Parameter	ITER	DEMO
Ha	6500	12,000
Re	30,000	60,000
Gr	7.0×10^9	2.0×10^{12}
Ha/Re	0.22	0.20
Gr/Re^2	7.8	5.6×10^2
Gr/Ha	1.1×10^6	1.7×10^8
$N = Ha^2/Re$	1.4×10^3	2.4×10^3

are the multi-channel effect owing to leaking currents between neighboring poloidal ducts (some new results for the DCLL concept are presented in Ref. [28]) and those due to spatial variations of the magnetic field and due to the existence of two other magnetic field components (*i.e.* poloidal and radial). Although small, these two field components may play a special role, especially if the flow turns out to be turbulent. Intensive three-dimensional disturbances will most likely occur at the locations where FCI boxes are overlapping and in the neighborhood of the pressure equalization openings in the FCI.

5. Fully developed flow model

In a fully developed flow, all flow variables do not vary with the axial coordinate x , except for the pressure P , which is a linear function of x , *i.e.* $dP/dx = \text{Const}$. Such flows are governed by the two equations for the axial velocity U and the induced magnetic field b_x , which are both functions of the toroidal z and the radial y coordinates:

$$\frac{\partial}{\partial z} \left((v + \nu_{tz}) \frac{\partial U}{\partial z} \right) + \frac{\partial}{\partial y} \left((v + \nu_{ty}) \frac{\partial U}{\partial y} \right) - \frac{1}{\rho} \frac{dP}{dx} + \frac{1}{\rho \mu_0} \left(B_z^0 \frac{\partial b_x}{\partial z} + B_y^0 \frac{\partial b_x}{\partial y} \right) = 0 \tag{1}$$

and

$$\frac{1}{\mu_0} \frac{\partial}{\partial z} \left(\frac{1}{\sigma_y} \frac{\partial b_x}{\partial z} \right) + \frac{1}{\mu_0} \frac{\partial}{\partial y} \left(\frac{1}{\sigma_z} \frac{\partial b_x}{\partial y} \right) + B_z^0 \frac{\partial U}{\partial z} + B_y^0 \frac{\partial U}{\partial y} = 0. \tag{2}$$

Here, B_z^0 and B_y^0 are the two components of the plasma-confining magnetic field, while μ_0 is the magnetic permeability, and ν_t is the turbulent (eddy) viscosity. In what follows the radial field component B_y^0 is neglected, since $B_y^0 \ll B_z^0$. Taking into account that in a strong magnetic field turbulence reaches its extremely anisotropic state with almost no variations of turbulence characteristics along

the magnetic field lines, one can put $\nu_{tz} = 0$, while the other viscosity component ν_{ty} needs to be modeled. Eq. (1) is applied to the liquid domain, including the bulk flow and that in the gap, while Eq. (2) covers the whole cross-sectional duct area, including the flow domain, the FCI, and the ferritic wall. Since Eq. (2) is written in a conservative form (σ is inside the derivative), inner boundary conditions on b_x are not needed. The outer boundary condition (at the external side of the ferritic wall) is $b_x = 0$. The above model can be applied to flows without volumetric heating, *i.e.* in the ITER H-H scenario, or under conditions when buoyancy-driven flows are insignificant compared with the forced flow. With some modification (after adding a buoyancy force term on the right-hand-side of the momentum equation and introducing the energy equation) the model can be extended to the analysis of fully developed buoyant flows.

6. Formation of high-velocity near-wall jets

Model equations (1) and (2) can be used to illustrate the mechanism of jet formation in the flow with the FCI (Fig. 5). The computations are performed with a finite-volume numerical code described in Ref. [29]. The flow is assumed to be laminar, *i.e.* $\nu_{ty} = 0$. The induced electric currents (Fig. 5a) flow almost radially (*i.e.* perpendicular to the magnetic field lines) in the core. In the two side boundary layers they turn slightly and then cross the two opposite flow insert plates at a right angle. Outside the FCI box, the currents flow almost tangentially in the ferritic wall and in the gap between the FCI and the structural wall. This electric current circuit is responsible for the flow opposing Lorentz force, which is higher in the core and lower in the vicinity of the parallel walls. As a result, a significant portion of the volumetric flow rate in the bulk flow is localized near the side walls in the form of two high-velocity near-wall jets (Fig. 5b). The velocity in the thin gap parallel to the applied magnetic field is comparable with that in the jets, while the flows in the two gap sections adjacent to the Hartmann walls are almost stagnant. The effect of the SiC electrical conductivity on the jets is

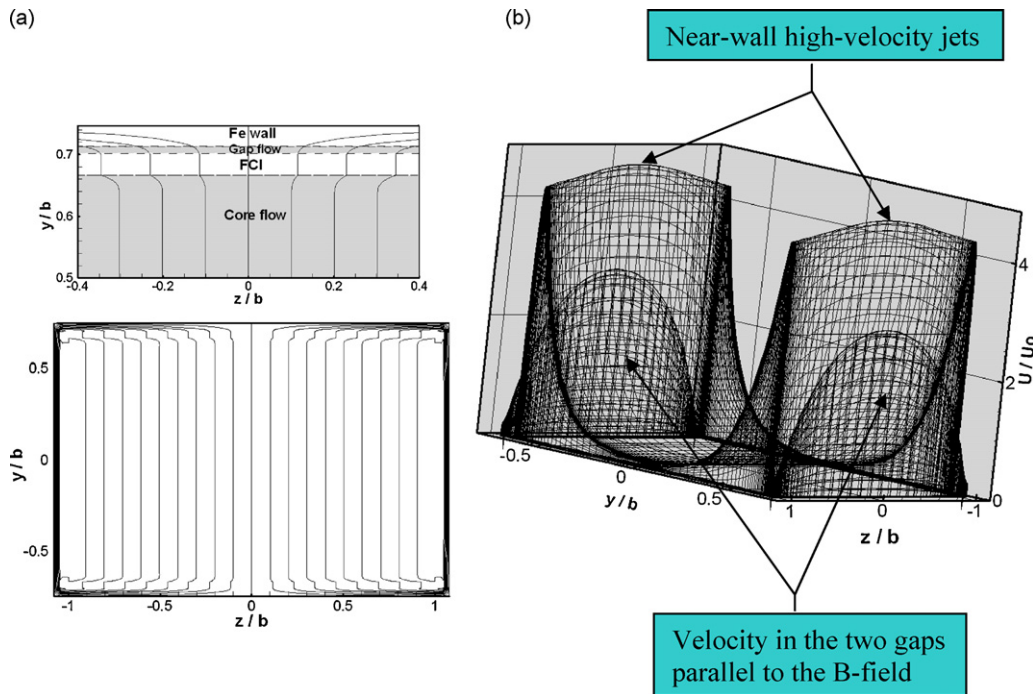


Fig. 5. Formation of high-velocity near-wall jets in the poloidal duct flow with the FCI (5 mm, $\sigma_{SiC} = 100 \text{ S/m}$): (a) induced magnetic field contour plot and (b) velocity distribution. Demo blanket conditions: $Ha = 15,900$; $b/a = 1.5$ [11].

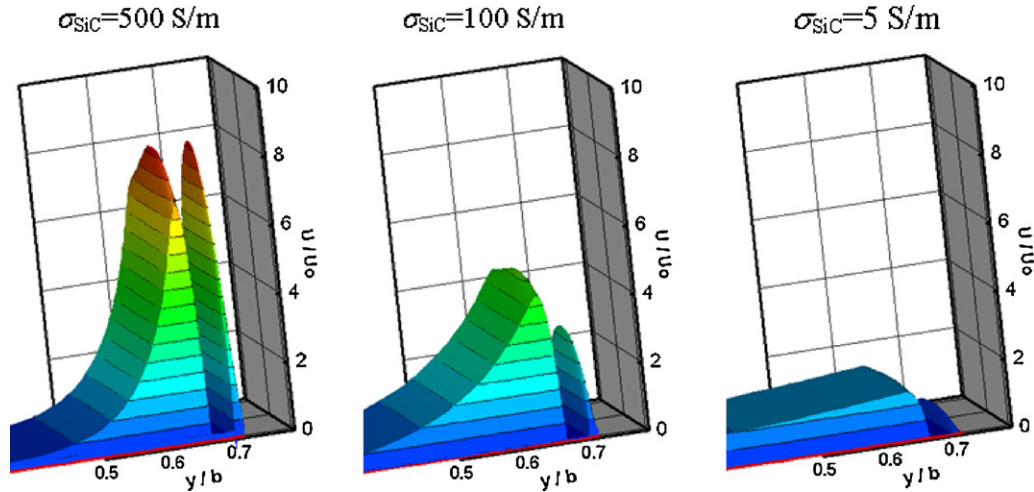


Fig. 6. Effect of the SiC electrical conductivity on the jet flow. See parameters in Fig. 5.

analyzed in Ref. [12] and illustrated here in Fig. 6. As the electrical conductivity decreases, the induced electric current decreases, resulting in more uniform velocity distribution and lower jet velocity. The jets have a tremendous effect on the temperature field [16]. Their remarkable feature is the existence of inflection points in regions where the velocity profile exhibits a strong velocity gradient. Under certain conditions, the internal shear layer associated with these inflection points is subject to Kelvin–Helmholtz (inflectional) instability, resulting in amplification of originally small flow perturbations, and eventually in Q2D turbulence (Section 10).

7. Jet modification in turbulent flows

If the bulk flow turns out to be turbulent the near-wall jets will be strongly affected by turbulent diffusion. Fig. 7 shows the effect of jet reduction in a turbulent flow computed with Eqs. (1) and (2) where the turbulent viscosity was calculated using the zero-

equation turbulence model derived in Ref. [14]. For the chosen set of the parameters, one can see a strong, about three times, reduction of the jet velocity and jet thickening compared to the laminar flow. At the same time the flow in the gap remains laminar; the maximum velocity of the flow in the gap section parallel to the magnetic field becomes significantly higher than that in the bulk flow. Despite the differences between the laminar and turbulent velocity profiles, the MHD pressure drop in the turbulent case is only slightly above the laminar value, indicating that the friction component of the pressure drop is much smaller than that due to the core Lorentz force, which is about the same in magnitude in both cases. This conclusion is in a good agreement with numerous experimental observations showing that in a strong magnetic field the flow exhibits turbulent fluctuations while the friction factor still obeys the laminar law (e.g. [30]). The reduction of the jet velocity and the increase of the effective thermal conductivity are both responsible for significant effects on the temperature distribution

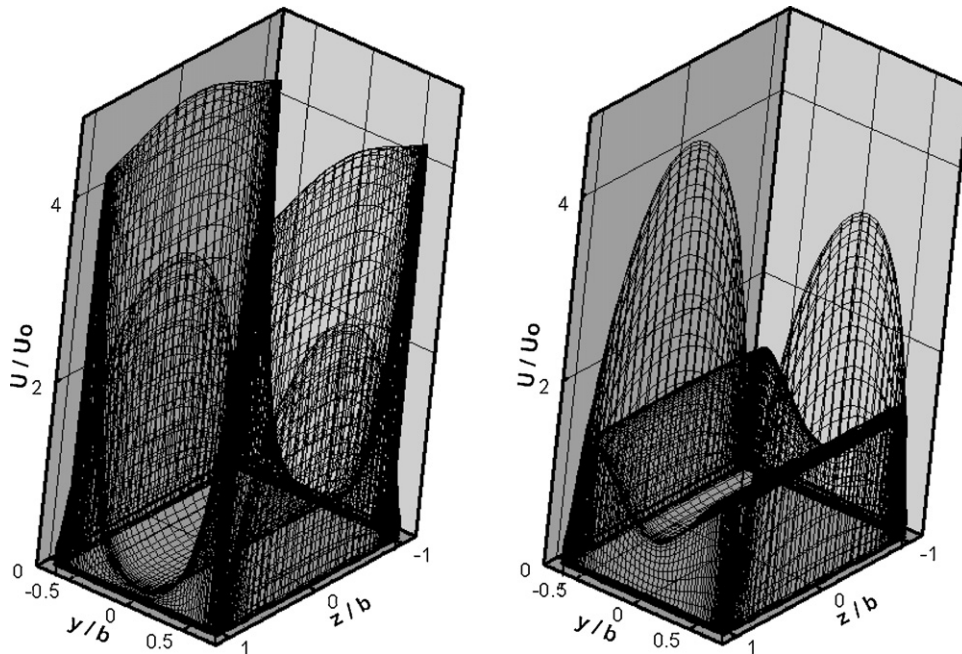


Fig. 7. Modification of the near-wall jet due to turbulent diffusion. The laminar velocity profile (left) is compared with the turbulent profile (right) at $Re=60,000$. See parameters in Fig. 5.

in the DCLL blanket, namely for more uniform temperature profiles in the radial direction, as demonstrated via numerical simulations in Ref. [16].

8. Laminar to turbulent transition under blanket conditions

Whether the flow is laminar or turbulent is an important issue, since the choice of a proper flow model will definitely affect the accuracy of the theoretical predictions. Although, for ordinary flows, justification of the flow regime in ducts is relatively simple (based on the comparison of the Reynolds number with its critical value), a single parameter characterizing transition from a laminar MHD flow to Q2D turbulence in rectangular ducts does not exist. Unlike ordinary flows, in MHD, transitions to turbulence typically occur in internal shear layers [29]. The formation of such layers can be affected by various parameters and flow conditions, including the magnetic field strength and its spatial distribution, electrical conductivity of the walls, and the duct aspect ratio. However, the existence of the shear layers itself does not guarantee the flow to be turbulent. A mechanism preventing the shear layers from being unstable and ultimately turbulent is the energy dissipation that includes viscous losses, which occur mostly in the Hartmann layers, and ohmic losses associated with closing the electric current in both Hartmann layers and electrically conducting walls. The role of the Hartmann number (as the basic dimensionless parameter that stands for the magnetic field strength) in the transitions is therefore twofold. On the one hand, the formation of potentially unstable velocity profiles with inflection points occurs in flows where the Hartmann number is sufficiently high. A typical example is the MHD flow in a thin-walled rectangular duct in a strong uniform transverse magnetic field, where turbulence generation is associated with the well-known M-shaped velocity profile. On the other hand, once the flow becomes unstable and ultimately turbulent, dissipation losses in the perturbed flow increase as the Hartmann number increases. Therefore turbulence appearance and its self-sustaining depend on two competing mechanisms, both related to the magnetic field strength. This is also true in the case of rectangular duct flows with the insulating flow insert. However, this case is more challenging for the analysis compared to the thin-walled ducts without insulation, since the electric currents generated by the flow exhibit a complicated path that involves the current distribution in the FCI and in the gap as shown in Section 6.

Additionally to the Hartmann number, another important parameter in the turbulent transitions is the ratio of the electrical conductivity of the flow-confining structure and that of the flow. In the particular case of thin conducting walls without electrical insulation, such a parameter reduces to the well-known wall conductance ratio $c_w = t_w \sigma_w / (b\sigma)$, where σ_w denotes the electrical conductivity of the wall and t_w is the wall thickness. The wall conductance ratio has a strong effect both on the dissipation losses and the shape of the velocity profile in MHD flows in rectangular ducts, thus controlling turbulence generation or its damping. Depending on c_w , the dissipation losses are known to vary as Ha in ducts with insulating walls or as Ha^2 in electrically conducting ducts (e.g. [32]).

The role of electrically conducting walls in turbulence transitions can further be illustrated with a simple analysis for a Q2D flow between two plane electrically conducting walls in a uniform wall normal magnetic field. Two time scales can be used to characterize the lifetime of turbulent structures in such a flow: (i) the Hartmann braking time, which is the characteristic time of damping due to both ohmic and viscous energy dissipation (e.g. [32]):

$$\tau = \frac{b^2}{\nu} \frac{1}{Ha} \frac{1}{1 + c_w Ha / (1 + c_w)} \quad (3)$$

and (ii) the turnover time of the large energy-containing eddies, related to the non-linear mechanism of the energy redistribution between the mean-flow and turbulent pulsations. Denoting the characteristic size of large eddies l^* and their velocity U^* , the condition of low turbulence damping is therefore given by $l^*/U^* \ll \tau$, or

$$\frac{Re_*}{Ha} \left(\frac{b}{l^*} \right)^2 \frac{1}{1 + c_w Ha / (1 + c_w)} \gg 1. \quad (4)$$

The subscript “star” indicates that the Reynolds number Re_* is built using l^* and U^* .

For the estimation purposes, Eq. (4) can also be applied to thin-walled rectangular duct flows in the blanket conditions, where dissipation losses associated with the Hartmann layers and Hartmann walls are predominant. In turbulent Q2D rectangular duct flows, a typical large-eddy size is comparable with the duct dimension: $l^* \sim a$ (e.g. [23]), and $U^* \sim U_0$, so that $Re_* \sim Re$. If the Hartmann walls are highly conducting ($c_w Ha \rightarrow \infty$), condition (4) transforms to

$$\frac{1}{c_w} \frac{Re}{Ha^2} \left(\frac{b}{a} \right)^2 \gg 1,$$

suggesting that in the electrically conducting blanket, where Re and $Ha \sim 10^4$, $b/a \sim 1$, and $c_w \sim 0.1$, turbulence does not appear and self-sustain. If so, the induced currents associated with the turbulent eddies are closed through the walls, resulting in fast turbulence damping, which occurs at the Joule timescale:

$$\tau = \tau_j = \frac{\rho}{\sigma B_0^2}. \quad (5)$$

On the other hand, if the walls are perfectly insulating ($c_w = 0$) or poor conducting ($c_w Ha \ll 1$) condition (4) can easily be satisfied and existence of self-sustained Q2D turbulence is possible. In this case, the electric currents induced in the core are closed through the Hartmann layers, which have relatively high electrical resistance. The braking time becomes

$$\tau = \tau_j Ha = \frac{b(\rho/\sigma_1\nu)^{1/2}}{B_0} = \frac{Ha^{-1}b^2}{\nu}, \quad (6)$$

which is many orders of magnitude higher than the Joule time scale.

It should be mentioned that formulas (3)–(6) are not in a full quantitative agreement with experimental data for a thin-walled duct [34], which show pronounced fluctuations, although no turbulence is predicted with (4). This discrepancy may indicate that criterion (4), which is purely local, cannot be sufficient to yield a general rule for the existence of turbulence in flows as complex as those in the blanket ducts even in the particular case of no insulation.

As applied to the DCLL blanket with the insulating flow insert, turbulence is likely to appear and self-sustain in a certain range of the FCI thickness and its electrical conductivity. Namely, insulating properties of the FCI may favor the situation when the potentially unstable M-shaped velocity profile is formed while the induced currents are sufficiently reduced, providing conditions when turbulence production and its dissipation are in balance. The physical basis for deriving a proper transition criterion in these conditions is still the same: the comparison between the eddy turnover time and the braking time. The latter, however, needs a special analysis of the induced current path and its impact on the energy losses in the flow, which in the case with the FCI is still missing.

9. Unsteady flow model with convection and buoyancy force

For many years MHD flows under the LM blanket conditions have been treated under stationary inertialess approximations, since it was expected that time-dependent inertial flows would be suppressed by a strong magnetic field (e.g. [32]). Although the inertial effects are often insignificant with regard to the overall pressure losses, they can be important from the point of view of their impact on the velocity field and, through velocity changes, on heat transfer. The importance of inertia terms for the full unsteady analysis of the blanket flows has been recognized only recently [33].

In a strong magnetic field, flow disturbances along the magnetic field lines tend to be inhibited by the action of the magnetic field due to a kind of “magnetic diffusion” [24] and a Q2D flow is promoted. In the analysis of this kind of flows in rectangular ducts it is usual to split the flow into the core and the Hartmann and side layers (e.g. [32]). In a strong transverse magnetic field, the Hartmann layers are very thin ($O(Ha^{-1})$) and, because inertia is negligible, can be treated explicitly. In turn, the core velocity presents no variation along the magnetic field lines. These allow integrating (averaging) the governing equations along the magnetic field lines resulting in two-dimensional equations, in which a new linear friction term, usually quoted as the Hartmann damping, appears. With the averaged equations, the computational effort of solving the original three-dimensional problem is sufficiently reduced. Such an approach, originally established by Sommeria and Moreau [24] in the context of turbulent flows in ducts with insulating walls, has been extended and successfully applied to a number of MHD duct flows [35–37]. We also follow this approach here to address such blanket-related phenomena as Q2D turbulence (Section 10) and buoyancy effects (Section 11).

To extend this approach to buoyancy-driven flows in the ITER-D-T or DEMO scenario, we assume that buoyancy effects are present due to non-uniform bulk heating \dot{q} , which is approximated here with the following formula:

$$\dot{q}(y) = q_0 e^{-(y+a)/l},$$

where the ratio $a/l \equiv m$ is hereafter referred to as the “shape parameter”. After integrating the governing equations in the z -direction along the magnetic field lines, the set of equations formulated in terms of the velocity components U and V , pressure P , and temperature T , all depending on the coordinates x and y in the plane perpendicular to the applied magnetic field, takes the following form:

$$\frac{\partial U}{\partial t} + U \frac{\partial U}{\partial x} + V \frac{\partial U}{\partial y} = -\frac{1}{\rho} \frac{\partial P}{\partial x} + \nu \left(\frac{\partial^2 U}{\partial x^2} + \frac{\partial^2 U}{\partial y^2} \right) - \frac{U}{\tau} + g(-1)^n + g(-1)^n \beta(T_0 - T), \quad (7)$$

$$\frac{\partial V}{\partial t} + U \frac{\partial V}{\partial x} + V \frac{\partial V}{\partial y} = -\frac{1}{\rho} \frac{\partial P}{\partial y} + \nu \left(\frac{\partial^2 V}{\partial x^2} + \frac{\partial^2 V}{\partial y^2} \right) - \frac{V}{\tau}, \quad (8)$$

$$\frac{\partial U}{\partial x} + \frac{\partial V}{\partial y} = 0, \quad (9)$$

$$\rho C_p \left(\frac{\partial T}{\partial t} + U \frac{\partial T}{\partial x} + V \frac{\partial T}{\partial y} \right) = k \left(\frac{\partial^2 T}{\partial x^2} + \frac{\partial^2 T}{\partial y^2} \right) + \dot{q}. \quad (10)$$

As applied to a poloidal blanket, z denotes the toroidal coordinate, while x and y stand for the poloidal and radial coordinates correspondingly; t is the time, C_p is the specific heat, and T_0 is the

inlet temperature in the liquid. The x -axis coincides with the duct axis and the origin is located at the flow inlet as shown in Fig. 9. Parameter $n=1$ on the right-hand-side of Eq. (7) corresponds to buoyancy-assisted flows (forced flow is upwards), while $n=2$ to buoyancy-opposed flows (forced flow is downwards). In Eqs. (7) and (8) there is a term linear in the velocity, which includes the Hartmann braking time τ introduced earlier. In the particular case considered here for buoyant flows, we assume near-perfect electrical insulation by FCI, so that the Hartmann braking time is given by Eq. (6). As shown in Refs. [12,13], near-perfect electrical insulation can be achieved in both ITER and DEMO blanket conditions using a 5 mm FCI with the electrical conductivity of 1 S/m or less.

10. Q2D MHD turbulence

Unlike homogeneous MHD turbulence dominated by the development of the anisotropy due to Joule effect [31], in the Q2D MHD turbulent flows, three-dimensional effects and most of ohmic and viscous losses occur only in the thin Hartmann layers, while the bulk flow is essentially two-dimensional. The turbulent structures appear as big (comparable in size to the duct dimension) columnar-like vortices with their axis aligned with the magnetic field direction. Such Q2D eddies do not induce much electric current and thus are weakly affected by the magnetic field. They persist over many eddy turnovers, until being damped via slow dissipating processes in the Hartmann layers. As applied to a poloidal LM blanket, the Q2D turbulent eddies are expected to intensify radial heat and mass transport as recent experimental studies show [34], whereas their effect on the pressure drop is known to be insignificant. As shown in Section 7 of the present paper, Q2D turbulence in blanket flows with the FCI can result in thickening the near-wall jets and reducing the maximum jet velocity at the same time. This has been demonstrated using the zero-equation model, which belongs to the group of RANS (Reynolds-averaged Navier–Stokes) equations, which due to their nature do not reproduce the internal turbulence structure. Unlike Section 7, here, we present direct simulations of Q2D MHD turbulent flows to illustrate possible turbulent flow patterns in detail.

Typical vortical flow patterns in a Q2D MHD turbulent flow are computed in Ref. [14] using a Q2D model, where a new term modeling a spatially non-uniform volumetric force was added to simulate typical M-shaped velocity profiles. Fig. 8 shows DNS (direct numerical simulation) results that illustrate the vorticity distribution. Although these computations were performed at relatively low Re and Ha , the blanket flows should likely exhibit the same tendencies since the predominant dynamics remain essentially the same. The instability develops in the symmetric internal shear layers, resulting in a double row of counter-rotating vortices whose characteristic size is comparable with the duct dimension. The vortices are regularly distributed in space. However, significant irregularities in

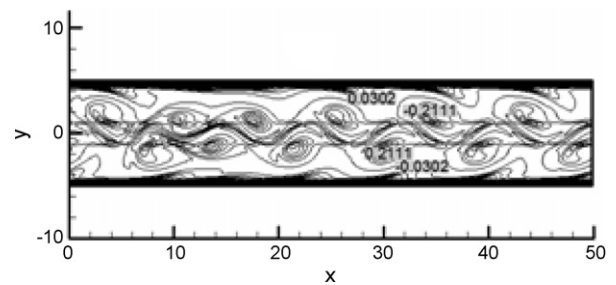


Fig. 8. Vorticity distribution in a Q2D turbulent MHD flow at $Re = 1000$ and $Ha = 500$ [14].

the flow can be observed in the form of “compound vortex islands,” where a few vortices group together to form a bigger coherent structure. This is clear evidence of Q2D turbulent flow dynamics, where “inverse energy cascade” occurs through merging vortices of about the same size to form a bigger one.

11. Mixed convection

In the blanket ducts in ITER D-T and DEMO, the forced flow is superimposed with the buoyant flow resulting in a mixed flow regime. Two characteristic temperature scales in the flow can be introduced: the radial temperature scale $\Delta T = \bar{q}a^2/k$ introduced earlier (Section 2), and the axial scale associated with the bulk temperature increase as the liquid moves poloidally from the inlet to the outlet. In the DCLL blanket conditions, the latter is sufficiently smaller. Therefore buoyancy effects in the liquid metal flow in the DCLL blanket are better characterized with the radial temperature scale associated with the non-uniform volumetric heating, whose intensity drops near exponentially in the radial direction, as shown in Fig. 4. To some degree buoyancy-driven flows in the DCLL blanket are similar to the classic case of differential heating when convective flows occur in a gap between two vertical walls, one of which is “hot” and the other is “cold,” so that the buoyancy force makes the liquid flow upwards near the hot wall and downwards near the opposite wall. Under the strong reactor magnetic field, the convective flows are again expected to be essentially Q2D, with 3D effects localized in the thin Hartmann layers. This striking feature allows for using the Q2D flow model described in Section 9. The effect of buoyancy forces on the blanket operation manifests itself through intensive thermal mixing, which can exhibit either laminar or turbulent features. The increase in the effective heat transfer coefficient (or Nusselt number) due to buoyancy effects may result in higher heat losses from the PbLi flow into the cooling helium streams and this

Table 2
Typical values of r and m in the poloidal flows of the DCLL blanket

Duct	m	r
DEMO #1 (front)	1.0	40
DEMO #2	0.25	12
DEMO #3	0.15	5
ITER D-T #1 (front)	0.3	10
ITER D-T #2	0.2	8

would degrade the thermal blanket efficiency. Such heat transfer intensification associated with turbulent natural convection in the presence of a transverse magnetic field has been demonstrated experimentally [38] and numerically [39]. Another concern associated with the buoyancy effects in the blanket is a risk of locally reverse (or recirculating) flows and associated “hot spots” and tritium accumulation, which may occur in the return ducts of the blanket module (Figs. 1 and 2) where the liquid flows downwards.

To access the important flow features, a number of simplifying assumptions are made: (i) the flow is laminar; (ii) the flow is fully developed; and (iii) all duct walls are perfectly insulating both electrically and thermally. The last assumption allows for Neumann thermal boundary conditions at the walls. The assumption (ii) is justified for long ducts, where the entry/exit effects can be neglected. This seems to be valid in the DCLL blanket conditions, where the ratio between the duct length and the characteristic cross-sectional dimension is typically high: 50 in ITER and 20 in DEMO. A few relevant cases have been simulated in Ref. [39] for natural convection, demonstrating that the edge sections with strong disturbances due to boundary conditions at the top and bottom are short. The validity of the fully developed flow assumption has, however, to be further checked via numerical simulations or experimentally in conditions of the real blanket design with pertinent flow parameters.

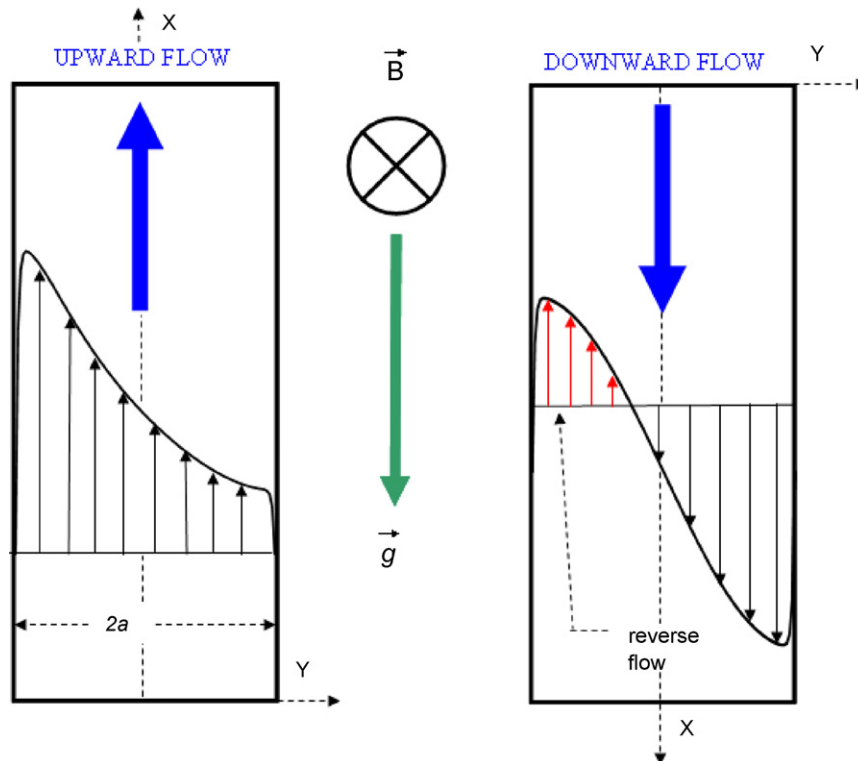


Fig. 9. Sketch illustrating the forced flow direction with respect to the gravity vector in the mixed convection problem.

Under the assumptions made, Eqs. (7)–(10) take the following form:

$$0 = -\frac{1}{\rho} \frac{dP}{dx} + \nu \frac{d^2U}{dy^2} - g(-1)^n g\beta(T - T_0) - \frac{U}{\tau}, \quad (11)$$

$$U \frac{\partial T}{\partial x} = \frac{k}{\rho C_p} \frac{\partial^2 T}{\partial y^2} + \frac{\dot{q}}{\rho C_p}, \quad (12)$$

where τ in the case of electrically insulating walls analyzed here is given by Eq. (6). The temperature and the pressure can be written in the following way:

$$T = T_0 + \gamma x + \theta(y), \quad (13)$$

$$P = P_0 - \rho[G - g(-1)^n]x - g(-1)^n \rho\beta\gamma \frac{x^2}{2}. \quad (14)$$

Here, T_0 and P_0 are the temperature and the pressure at the flow inlet. The two constants G and γ can be found from the global energy/mass balance. The special solution form (13) reflects the fact that without the heat losses and with the x -independent heat generation in the liquid, the bulk temperature is a linear function of x , so that $\theta(y)$ is responsible for the cross-sectional temperature variations imposed on the bulk temperature. The global energy balance thus requires $\int_{-a}^a \theta(y) dy = 0$ being satisfied. By integrating Eq.

(12) between the side walls and using (13) one can find

$$\gamma = \frac{1}{\rho C_p U_0} \bar{q}, \quad \text{where } \bar{q} \equiv \frac{1}{2a} \int_{-a}^a \dot{q} dy = \frac{q_0(1 - e^{-2m})}{2m}.$$

After substitution of expressions (13) and (14) into Eqs. (11) and (12) and writing the resulting equations in the dimensionless form, the following equations can be obtained:

$$\tilde{U}'' - Ha \left(\frac{a}{b}\right)^2 \tilde{U} - (-1)^n \frac{Gr}{Re} \tilde{\theta} = -G \frac{a^2}{\nu U_0}, \quad (15)$$

$$\tilde{U} - \tilde{\theta}'' = \frac{2m}{1 - e^{-2m}} e^{-m(\tilde{y}+1)}. \quad (16)$$

Here, the mean-flow velocity U_0 is used as the velocity scale, $[\theta] = \bar{q}a^2/k$ as the temperature scale, and a as the length scale. Tilde is used to mark dimensionless variables. The Hartmann and the Reynolds numbers are defined as before, and the Grashof number is $Gr = g\beta[\theta]a^3/\nu^2$. Eq. (15) can further be simplified by neglecting the second derivative \tilde{U}'' , because, at high Ha numbers, friction in the side layers is negligible in comparison with Hartmann damping. Besides, the side layers, which are very thin, do not carry any significant flow rate. After integrating the resulting equations between the side walls, the following expression for constant G is obtained:

$$G \frac{a^2}{\nu U_0} = Ha \left(\frac{a}{b}\right)^2.$$

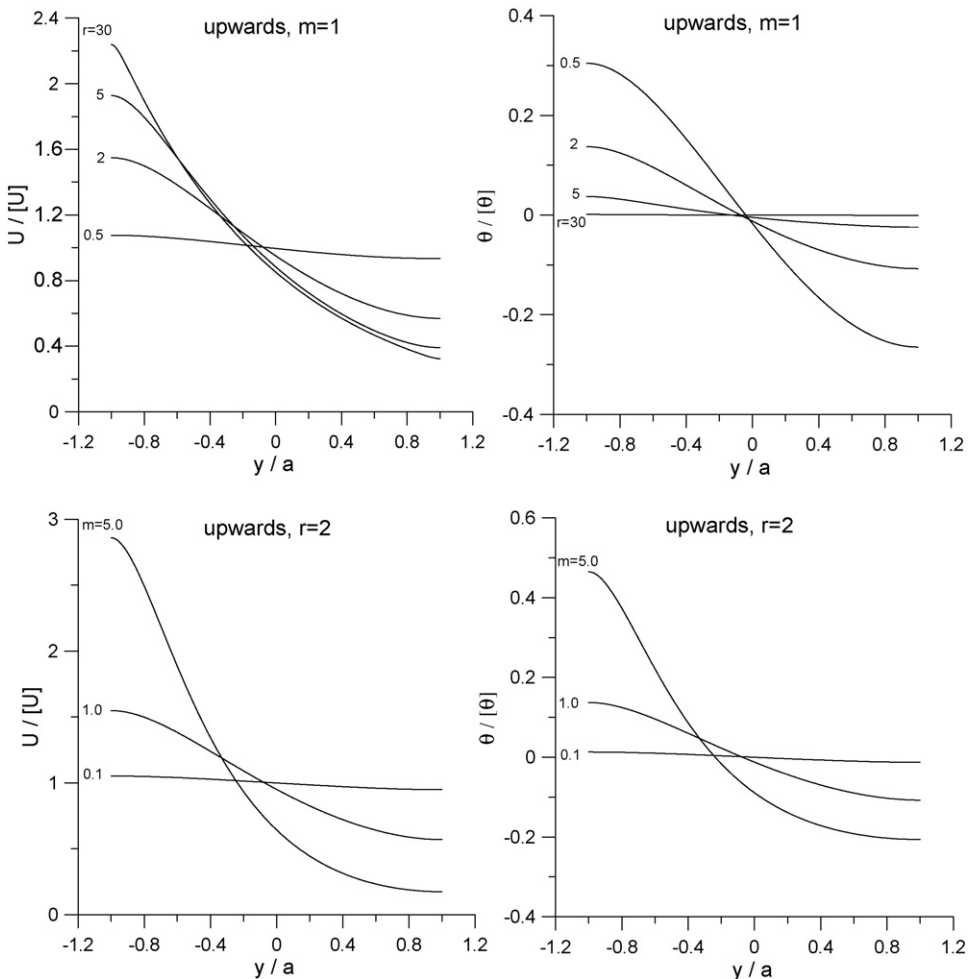


Fig. 10. Effect of r and m on mixed convection when the forced flow is upwards.

Finally, Eq. (15) takes a very simple form:

$$\tilde{U} = 1 - (-1)^n r^2 \tilde{\theta}, \tag{17}$$

where

$$r = \sqrt{\frac{Gr}{Ha Re(a/b)^2}} \tag{18}$$

is a new important dimensionless parameter. The solution of Eqs. (16) and (17) for the case of upward flow ($n=1$, Fig. 9 left) with adiabatic wall boundary conditions is as follows:

$$\theta(y) = \frac{\bar{q}a^2}{k} \left\{ \frac{2m^2}{r(r^2 - m^2)(1 - e^{-2m})} \left[\frac{e^{-2m} \cosh[r(y/a) + 1] - \cosh[r(y/a) - 1]}{\sinh(2r)} \right] + \frac{2m e^{-m(y/a+1)}}{(r^2 - m^2)(1 - e^{-2m})} - \frac{1}{r^2} \right\}, \tag{19}$$

$$U(y) = U_0 \left[1 + r^2 \frac{k}{\bar{q}a^2} \theta(y) \right]. \tag{20}$$

For the downward flow ($n=2$, Fig. 9 right) the solution is:

$$\theta(y) = \frac{\bar{q}a^2}{k} \left\{ -\frac{m^2}{r(r^2 + m^2)(1 - e^{-2m})} \left[\frac{\sin(r(y/a))(1 + e^{-2m}) + \cos(r(y/a))(1 - e^{-2m})}{\sin(r)} \right] - \frac{2m e^{-m(y/a+1)}}{(r^2 + m^2)(1 - e^{-2m})} + \frac{1}{r^2} \right\}, \tag{21}$$

$$U(y) = U_0 \left[1 - r^2 \frac{k}{\bar{q}a^2} \theta(y) \right]. \tag{22}$$

It is noticeable that there are only two dimensionless parameters, r and m , which enter the solution. The shape parameter m affects the steepness of the heating profile. It is fully determined by the

interaction of neutrons with the liquid metal. Parameter r , which combines Gr , Ha , Re and the aspect ratio a/b , is more related to the liquid metal flow itself as it carries information on the contribution of various forces acting on the flow, such as buoyancy, viscous, and electromagnetic forces. Its value is affected by the blanket operation parameters or/and duct dimensions. Typical values of r and m in the DCLL blanket for the current DEMO and ITER designs are summarized in Table 2, and their effect on mixed convection (based on the present analytical solutions) is demonstrated in Figs. 10 and 11.

In the upward flow case, higher velocity occurs at the “hot” wall, where volumetric heating reaches its maximum. The difference between the maximum velocity at the hot wall and the minimum

one at the cold wall increases with r approaching the asymptotic value when $r \gg 1$:

$$\frac{U_{\max} - U_{\min}}{U_0} = 2m. \tag{23}$$

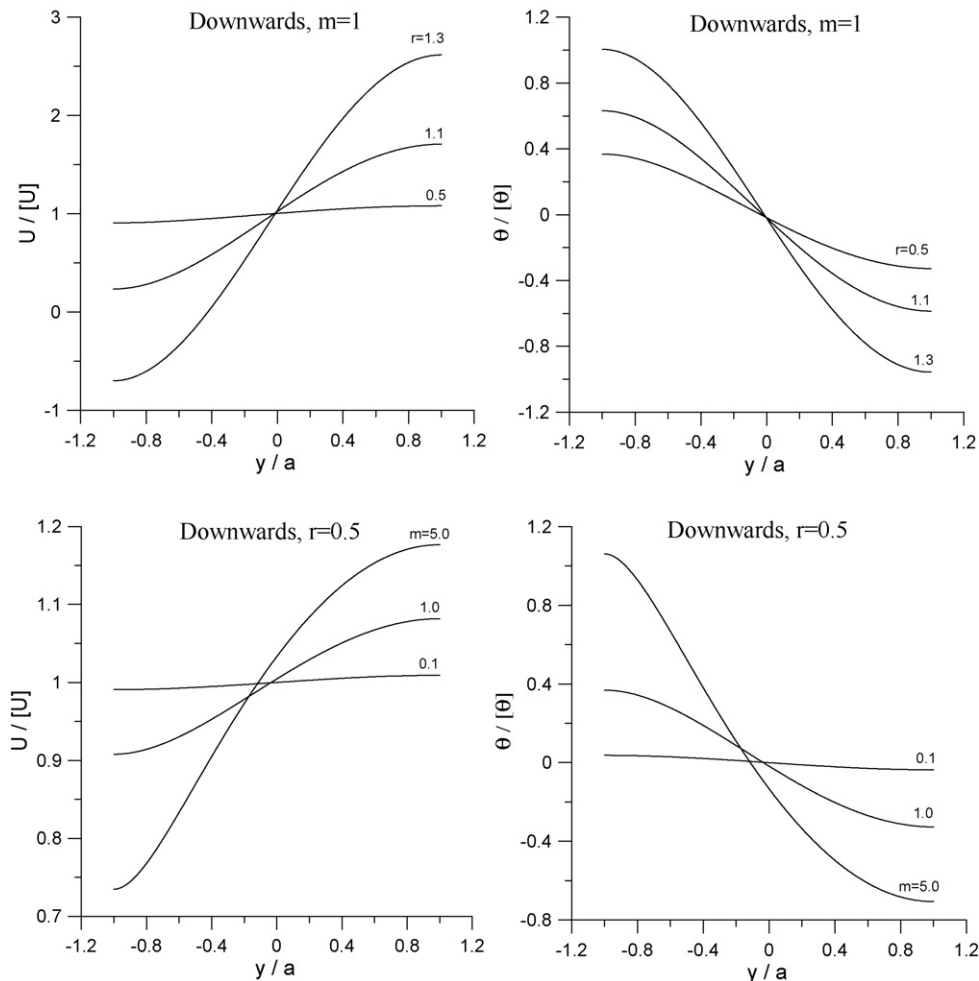


Fig. 11. Effect of r and m on mixed convection when the forced flow is downwards.

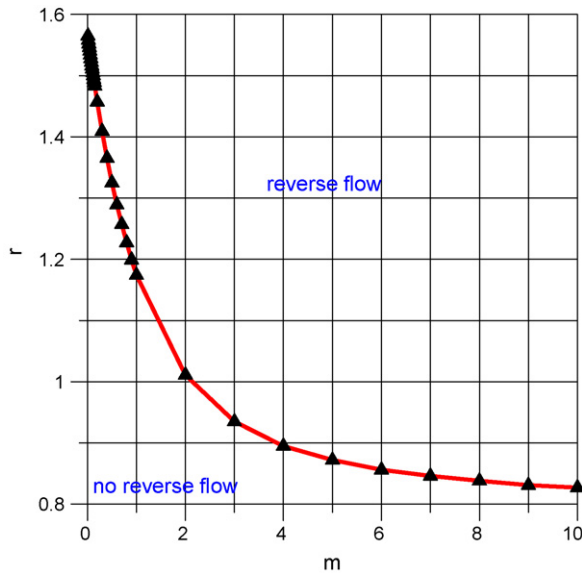


Fig. 12. Boundary curve in the r - m plane for downward flows.

At the same time the temperature profile becomes more and more uniform when r increases. In the case of the downward flow, both the velocity and temperature profiles become more non-uniform as r increases. At high enough r this tendency may result in a reverse flow near the hot wall where the buoyant and forced flows are opposite. The conditions where the reverse flow starts were found by solving equation $U(-a) = 0$ using formula (22). A corresponding boundary curve is shown in Fig. 12. It is noticeable that the present analysis suggests reverse flows in return ducts in both DEMO and ITER blankets. However, negative consequences of the reverse flows (e.g. through forming hot spots at the duct walls) are more likely in the DEMO conditions, where volumetric heating and operation temperatures are higher. It should be mentioned again that the present theory is limited to fully developed flows by neglecting edge effects at the top and bottom of the poloidal ducts. Therefore, real flows in the blanket can definitely be more complex than the current predictions. For example, reverse flows are likely to be modified due to inertia effects to a kind of recirculation flows. The advantage of the present theory is, however, in predicting conditions when the formation of such recirculation zones is possible by using simple analytical solutions.

12. Concluding remarks

Although the analysis done in this paper on MHD phenomena is not nearly enough to address all MHD blanket-related issues, it appears that important peculiarities of MHD flows in the DCLL blanket are related to the predominance of Q2D turbulence and convective effects. This differs from many previous considerations for other LM blankets where turbulence and convective effects were often neglected. The two special features that set off the DCLL concept from other LM blankets is (i) using a flow channel insert and (ii) running the LM flows at a moderate speed, which is much higher than that in the HCLL blanket, but at the same time significantly lower compared to a self-cooled blanket. The FCI has a finite electrical conductivity providing conditions where the electric currents induced in the LM flow can be significantly reduced but still leak outside the FCI structure. Such electric currents do not produce much dissipation, thus enabling self-sustained Q2D turbulence through the destabilization of the internal shear layers. On the other hand, the moderate flow velocity and intensive

volumetric heating are both favorable for the mixed flow regime, where buoyant flows can even dominate over the forced flow. When Q2D turbulence is combined with buoyant flows, new flow regimes can be foreseen. The resultant flow seems to be a very rich combination of phenomena, whose properties and the influence on the blanket operation are not very well understood yet. What limits the effectiveness of the studies is extremely large values of the dimensionless parameters: Ha , Re , and Gr . Although the separate effects can be addressed using simplified flow models, as those presented in this paper, studying the major multiple effects will require full modeling or prototypic physical experiments. In spite of a big challenge such studies are absolutely necessary in parallel with the design work for ITER TBM and R&D for the DEMO blanket, as MHD effects are of primary importance for the DCLL concept.

Acknowledgement

The study has been performed under DOE grant DE-FG02-86ER52123-A040.

References

- [1] G. Rampal, A. Li Puma, Y. Poitevin, E. Rigal, J. Szczepanski, C. Boudot, HCLL TBM for ITER-design studies, *Fusion Eng. Des.* 75–79 (2005) 917–922.
- [2] S. Malang, E. Bojarsky, L. Bühler, H. Deckers, U. Fischer, P. Norajitra, H. Reiser, Dual coolant liquid metal breeder blanket, in: *Proceedings of the 17th Symposium on Fusion Technology*, Rome, Italy, September 14–18, 1992, pp. 1424–1428.
- [3] D.L. Smith, C.C. Baker, D.K. Sze, G.D. Morgan, M.A. Abdou, S.J. Piet, S.R. Schultz, R.W. Moir, J.D. Gordon, Overview of the blanket comparison and selection study, *Fusion Technol.* 8 (1) (1985) 10–113.
- [4] S. Molokov, R. Moreau, H.K. Moffat (Eds.), *Magnetohydrodynamics. Historical Evolution and Trends*, Springer, 2007.
- [5] I.R. Kirillov, C.B. Reed, L. Barleon, K. Miyazaki, Present understanding of MHD and heat transfer phenomena for liquid metal blankets, *Fusion Eng. Des.* 27 (1995) 553–569.
- [6] N. Morley, S. Smolentsev, L. Barleon, I. Kirillov, M. Takahashi, Liquid magnetohydrodynamics—recent progress and future directions for fusion, *Fusion Eng. Des.* 51–52 (2000) 701–713.
- [7] N. Morley, S. Malang, I. Kirillov, Thermofluid magnetohydrodynamic issues for liquid breeders, *Fusion Sci. Technol.* 47 (2005) 488–501.
- [8] L. Bühler, Liquid metal magnetohydrodynamics for fusion blankets, in: S. Molokov, R. Moreau, H.K. Moffat (Eds.), *Magnetohydrodynamics. Historical Evolution and Trends*, Springer, 2007, pp. 171–194.
- [9] J. Reimann, L. Barleon, I. Buceniaks, L. Bühler, L. Lenhart, S. Malang, S. Molokov, I. Platnieks, R. Stieglitz, Magnetohydrodynamic investigations of a self-cooled Pb–17Li blanket with poloidal–radial–toroidal ducts, *Fusion Eng. Des.* 27 (1995) 593–606.
- [10] J. Reimann, L. Bühler, C. Mistrangelo, S. Molokov, Magneto-hydrodynamic issues of the HCLL blanket, *Fusion Eng. Des.* 81 (2006) 625–629.
- [11] S. Smolentsev, N. Morley, M. Abdou, R. Munipalli, R. Moreau, Current approaches to modeling MHD flows in the dual coolant lead lithium blanket, *Magnetohydrodynamics* 42 (2006) 225–236.
- [12] S. Smolentsev, N.B. Morley, M. Abdou, MHD and thermal issues of the SiC_f/SiC flow channel insert, *Fusion Sci. Technol.* 50 (2006) 107–119.
- [13] S. Smolentsev, M. Abdou, N.B. Morley, M. Sawan, S. Malang, C. Wong, Numerical analysis of MHD flow and heat transfer in a poloidal channel of the DCLL blanket with a SiC_f/SiC flow channel insert, *Fusion Eng. Des.* 81 (2006) 549–553.
- [14] S. Smolentsev, R. Moreau, Modeling quasi-two-dimensional turbulence in MHD duct flows, in: *Proceedings of the 2006 Summer Program*, CTR, Stanford University, 2006, pp. 419–430.
- [15] S. Smolentsev, R. Moreau, One-equation model for quasi-two-dimensional turbulent magnetohydrodynamic flows, *Phys. Fluids* 19 (2007) 078101.
- [16] S. Smolentsev, N.B. Morley, C. Wong, M. Abdou, MHD and heat transfer considerations for the US DCLL blanket for DEMO and ITER TBM, in: *ISFNT-8*, Heidelberg, Germany, September 30–October 5, 2007.
- [17] D.K. Sze, M. Tillack, L. El-Guebaly, Blanket system selection for the ARIES-ST, *Fusion Eng. Des.* 48 (2000) 371–378.
- [18] C.P.C. Wong, S. Malang, M. Sawan, M. Dagher, S. Smolentsev, B. Merrill, M. Youssef, S. Reyes, D.K. Sze, N.B. Morley, S. Sharafat, P. Calderoni, G. Sviatoslavsky, R. Kurtz, P. Fogarty, S. Zinkle, M. Abdou, An overview of dual coolant Pb–17Li breeder first wall and blanket concept development for the US ITER-TBM design, *Fusion Eng. Des.* 81 (2006) 461–467.
- [19] C.P.C. Wong, S. Malang, M. Sawan, S. Smolentsev, S. Majumdar, B. Merrill, D.K. Sze, N. Morley, S. Sharafat, M. Dagher, P. Peterson, H. Zhao, S.J. Zinkle, M. Abdou, M. Youssef, Assessment of first wall and blanket options with the use of liquid breeder, *Fusion Sci. Technol.* 47 (2005) 502–509.
- [20] ARIES Team M.S. Tillack, X.R. Wang, J. Pulsifer, S. Malang, D.K. Sze, ARIES-ST breeding blanket design and analysis, *Fusion Eng. Des.* 49–50 (2000) 689–695.

- [21] H. Branover, *Magnetohydrodynamic Flows in Ducts*, Wiley, New York, 1978.
- [22] R.G. Lingwood, T. Alboussière, On the stability of the Hartmann layer, *Phys. Fluids* 11 (1999) 2058–2068.
- [23] K. Messadek, R. Moreau, An experimental investigation of MHD quasi-two-dimensional turbulent shear flows, *J. Fluid Mech.* 456 (2002) 137–159.
- [24] J. Sommeria, R. Moreau, Why, how and when MHD turbulence becomes two-dimensional? *J. Fluid Mech.* 118 (1982) 507–518.
- [25] L. Bühler, Magnetohydrodynamic flows in arbitrary geometries in strong, nonuniform magnetic fields, *Fusion Technol.* 27 (1995) 3–24.
- [26] N.B. Morley, M.-J. Ni, R. Munipalli, M. Abdou, MHD simulations of liquid metal flow through a toroidally-oriented manifold, Heidelberg, Germany, September 30–October 5, 2007.
- [27] M.-J. Ni, R. Munipalli, N.B. Morley, P. Huang, M. Abdou, A current density conservative scheme for incompressible MHD flows at a low magnetic Reynolds number. Part I. On a rectangular collocated grid system, *J. Comp. Phys.* 227 (2007) 174–204.
- [28] C. Mistrangelo, A.R. Raffray, ARIES Team, MHD analysis of dual coolant Pb–17Li blanket for ARIES-CS, *Fusion Sci. Technol.* 52 (2007) 849–854.
- [29] S. Smolentsev, N. Morley, M. Abdou, Code development for analysis of MHD pressure drop reduction in a liquid metal blanket using insulation technique based on a fully developed flow model, *Fusion Eng. Des.* 73 (2005) 83–93.
- [30] A.B. Tsinober, Magnetohydrodynamic turbulence, *Magnetohydrodynamics* 11 (1975) 5–17.
- [31] B. Knaepen, R. Moreau, Magnetohydrodynamic turbulence at low magnetic Reynolds number, *Annu. Rev. Fluid Mech.* 40 (2008) 25–45.
- [32] U. Müller, L. Bühler, *Magnetohydrodynamics in Channels and Containers*, Springer, Berlin, 2001.
- [33] L. Bühler, Instabilities in quasi-two-dimensional magnetohydrodynamic flows, *J. Fluid Mech.* 326 (1996) 125–150.
- [34] U. Burr, L. Barleon, U. Müller, A.B. Tsinober, Turbulent transport of momentum and heat in magnetohydrodynamic rectangular duct flow with strong side wall jets, *J. Fluid Mech.* 406 (2000) 247–279.
- [35] I.V. Lavrent'ev, S.Yu. Molokov, S.I. Sidorenkov, A.R. Shishko, Stokes flow in a rectangular magnetohydrodynamic channel with nonconducting walls within a nonuniform magnetic field at large Hartmann numbers, *Magnetohydrodynamics* 26 (1990) 328–338.
- [36] S. Smolentsev, Averaged model in MHD duct flow calculations, *Magnetohydrodynamics* 33 (1997) 42–47.
- [37] S. Cuevas, S. Smolentsev, M. Abdou, On the flow past a magnetic obstacle, *J. Fluid Mech.* 553 (2006) 227–252.
- [38] T. Tagawa, G. Authié, R. Moreau, Buoyant flow in long vertical enclosures in the presence of a strong horizontal magnetic field. Part 1. Fully-established flow, *Eur. J. Mech. B* 21 (2002) 383–398.
- [39] G. Authié, T. Tagawa, R. Moreau, Buoyant flow in long vertical enclosures in the presence of a strong horizontal magnetic field. Part 2. Finite enclosures, *Eur. J. Mech. B* 22 (2003) 203–220.